2019

Liquid Crystal Elastomer Waveguide Actuators

Alexa S. Kuenstler
University of Massachusetts Amherst

Hyunki Kim
University of Massachusetts Amherst

Ryan C. Hayward
University of Massachusetts Amherst, hayward@umass.edu

Kuenstler, Alexa S.; Kim, Hyunki; and Hayward, Ryan C., "Liquid Crystal Elastomer Waveguide Actuators" (2019). *Advanced Materials*. 5.
https://doi.org/10.1002/adma.201901216

Liquid Crystal Elastomer Waveguide Actuators

*Alexa S. Kuenstler, Hyunki Kim, and Ryan C. Hayward**

A.S. Kuenstler, H. Kim, Prof. R.C. Hayward
Department of Polymer Science and Engineering, University of Massachusetts, Amherst, MA 01003, USA
Email: hayward@umass.edu

Keywords: liquid crystal elastomers, actuators, photoresponsive materials

Abstract

While most photomechanical materials developed to date have relied on free-space illumination to drive actuation, this strategy fails when direct line-of-site access is precluded. In this study, waveguided light is harnessed by liquid crystal elastomer (LCE) nanocomposites to drive actuation. Using photo-chemical reduction of gold salts to plasmonic nanoparticles, prescription of photoresponsive regions within fibers of mono-domain LCEs is demonstrated with control over both the location along the fiber axis, as well as in the azimuthal direction. Due to localized photothermal heating due to plasmonic absorption of waveguided light and resulting inhomogeneous thermally-induced deformation of the LCE, reversible bending along multiple axes is demonstrated.

Photomechanical actuators convert light into work through photochemical or photothermal effects.[1] Compared to other actinic stimuli including electric fields, magnetic fields, and chemical energy, light represents a particularly desirable mode of control because it can be spatiotemporally patterned and delivered over long distances with specified wavelength and polarization. Actuation in photochemical systems most commonly relies on changes in molecular ordering in a solid matrix due to unimolecular or bimolecular reactions, examples of which include isomerization of azobenzene in liquid crystal networks (LCNs)[2–6] and cycloadditions in molecular crystals.[7,8]

However, photochemical actuators often display slow actuation times limited by the time needed to accumulate sufficient product populations[9,10] and often require the use of multiple wavelengths to trigger forward and backward responses. In contrast, photothermal actuators often display rapid actuation, at least on mm- to cm-scales, as determined by heat transfer kinetics, and show highly reversible responses with only a single wavelength of light. Examples include plasmonic nanoparticles, dyes, and carbon allotropes loaded in gels,[11,12] thermoplastics,[13,14] and LCNs.[15–17]

Typically, free-space illumination is used to trigger actuation in photomechanical devices, which limits the utility of these devices to scenarios where direct and constant line-of-sight access is available. To overcome these limitations, waveguiding can be used to efficiently transport light over long distances and within arbitrary geometries. Despite these advantages, there are relatively few examples in the literature that couple waveguided light to photomechanical actuators.[18] Kuzyk's group has studied the deformation of azobenzene dye-doped poly(methyl methacrylate) (PMMA) optical fibers for use in interferometer applications.[19–22] In another example, Otani and co-workers constructed a micromanipulator using black dye on beveled polymer optical fibers to localize photothermal expansion.[23,24] However, deflection of these systems is modest (< 1º). Photoactive waveguides based on inorganic materials have also been demonstrated,[25] though these are also limited to small deflection angles. Actuation into a more complex shape was demonstrated by Small, *et al.* who used a shape memory polymer doped with a near-infrared (NIR) absorbing dye to drive irreversible actuation into a coil upon light absorption.[26] More recently, Zhou, *et al.* demonstrated reversible bending by up to 50º using poly(*N*-isopropylacrylamide) (PNIPAM) hydrogel nanocomposites loaded with gold nanoparticles.[27] While these examples

show the promise of waveguided light as an actuating stimulus, reversible bending along multiple directions with large deflection angles has not previously been possible.

In this work, we demonstrate a strategy for fabricating liquid crystal elastomer (LCE) fibers containing patterned regions doped with gold nanoparticles (AuNPs) to drive photothermal deformation in response to waveguided visible light. While thermal actuation[28–31] and unidirectional photoactuation[32–34] of LCE fibers has been previously demonstrated, to our knowledge this is the first demonstration of using these materials as actuating waveguides. Photoreduction of gold salt is used to localize deformation to specific "hinge" regions to achieve articulation in three-dimensions. With this platform, we demonstrate bending by up to 14º at a single actuator and incorporate as many as three hinges with independently patterned bending characteristics in a single cm-scale fiber for complex and reversible shape changes on a timescale of several seconds.

To fabricate a thermally-responsive fiber we relied on a dual-cure LCE platform developed by Yakacki and coworkers.[35,36] As illustrated in **Figure 1**a, a loosely-crosslinked fiber preform was fabricated via gelation in a cylindrical mold. Following gelation, pre-forms were placed under 200% tensile strain to align the director along the long axis of the fiber and cross-linked under UV light to form a nematic monodomain with a Young's modulus of ≈ 1 MPa, as characterized in a previous report.[36] To formulate a fiber that allowed for spatiotemporal control over photo-induced bending we sought a method to incorporate photoresponsive moieties in discrete regions along the fiber. While photothermal dyes have been previously exploited as photoresponsive

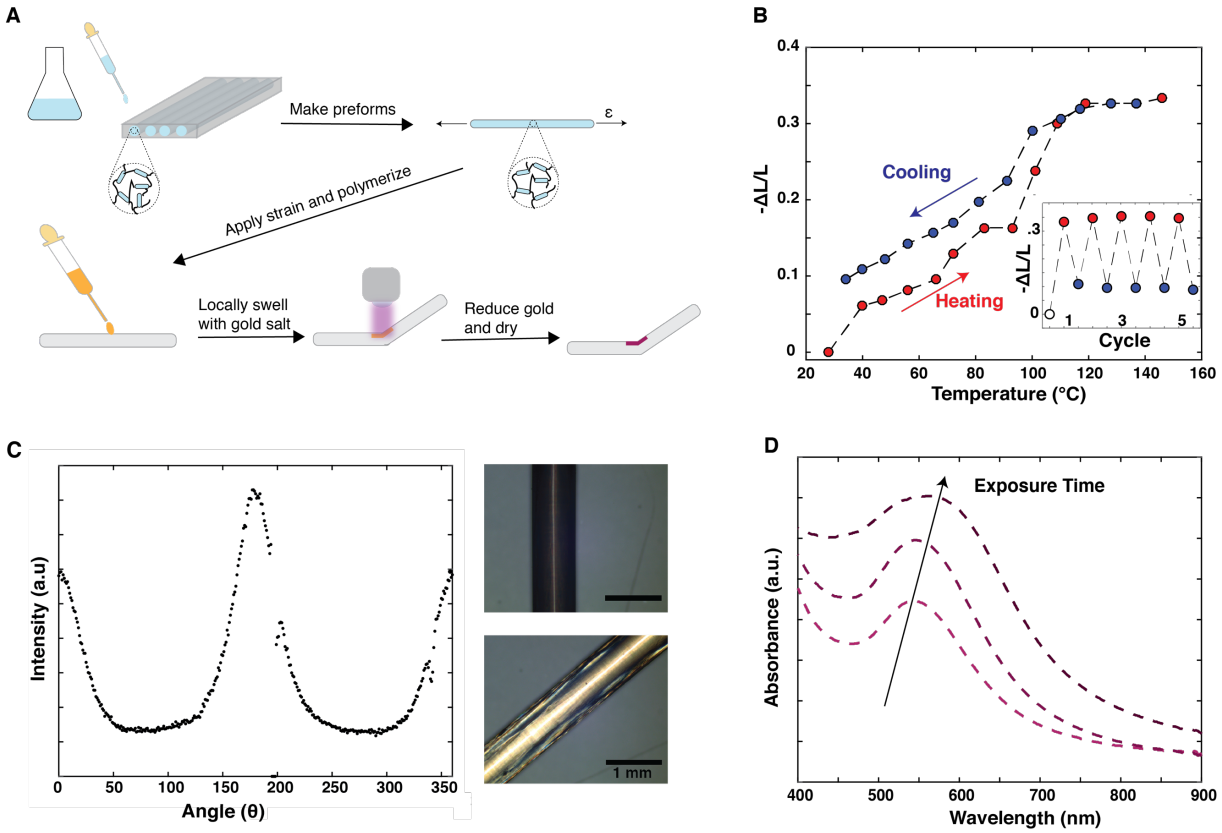

Figure 1. A) Polydomain LCE preforms are made via thiol-Michael addition in a silicone mold and aligned by photopolymerizing excess acrylate groups under strain. Gold solution is deposited on the surface of the fiber and allowed to locally swell the fiber before UV photoreduction for in situ nanoparticle formation. B) Fibers show > 30% contraction along their long axis upon heating (black circles) but only partially re-elongate after subsequently cooling (white circles). After the first heating cycle, ≈ 25% strain is reversible over several cycles (inset). C) The crosslinked fibers demonstrate good alignment as demonstrated by WAXS (left) and birefringence between crossed polarizers (right). D) Following UV exposure, strong absorbance at 530 nm is measured by UV-vis spectroscopy, indicating formation of gold nanoparticles. As the exposure time is increased, stronger absorbance is observed due to growth of the nanoparticles.

hinges[37], we decided to use AuNPs, which have significantly higher absorbance and photothermal efficiency than comparable dyes due to the large absorption cross-section provided by their surface plasmon resonance (SPR). To ensure uniform incorporation and limit aggregation of particles, within a spatially-controlled region, we chose photoreduction of gold salt.

Photochemical reduction of Au^{3+} ions to Au^0 metals by radical species has been demonstrated both in solution[38] and solid matrices[39]. Typical processes employ photoinitiatiors that generate ketyl radicals because of their high redox potentials.[40] We adapted this approach by using oleylamine in addition to $HAuCl_4$ and a ketyl-based UV photoinitiator. The oleylamine serves two purposes: 1) to initially reduce the gold partially, so that shorter UV exposure times can be employed and 2) to coordinate the gold particles and stabilize them in the polymer matrix.[41–43] A 1 μL droplet of the gold precursor solution was deposited on the surface of a pre-aligned fiber in the desired region and allowed to locally swell the LCE. After swelling, the fiber was exposed to UV light focused on its surface to drive formation of nanoparticles. Finally, the solvent was removed under vacuum to yield a patterned device. Following solvent removal, the fiber retained a bend where swelling occurred due to a slight decrease in the order parameter from 0.34 to 0.27. We hypothesize that this decrease is due to molecular memory of the initial, lightly crosslinked polydomain state. It is well-established that in double networks there is a competition between the elastic restoring force of the first network and the imposed strain of the second network.[44,45] While the second stage crosslinking locks in a monodomain, a fiber cycled above and below T_{NI} never returns to its full initial length. Instead, the fiber selects an equilibrium length at room temperature that is slightly shorter than the length following photocrosslinking which the fiber returns to on each subsequent cycle (**Figure 1**b). This indicates that the network reaches a state that balances the restoring force of the first network towards a polydomain and the nematic ordering of the second network that forces the polymer chains to be extended along the long axis of the fiber.

The final devices had a diameter of d = 700—800 μm and were cut to the desired length using a razor blade. Following crosslinking, the fibers had a measured order parameter of 0.34 and were

observed to undergo ≈ 25% reversible strain upon heating and cooling (see **Figure 1**b-c). Formation of AuNPs was confirmed by ultraviolet-visible (UV-vis) spectroscopy, where a strong absorbance at 530 nm was observed that corresponds to the surface plasmon resonance (SPR) of spherical particles (**Figure 1**d). Additionally, the absorbance increased with exposure time, providing a simple means to specify the optical density of each nanocomposite region independently.

To evaluate the photoactuation of the patterned nanocomposite fibers, a 532 nm diode pumped solid state (DPSS) laser was used. First, the response under free-space illumination was evaluated by shining the laser onto the nanoparticle-loaded region. The fiber was observed to bend at the hinge region, towards the side patterned with AuNPs, within a few seconds (see Supplementary Information). Because the AuNPs are localized to near one side of the fiber, the temperature rise is greatest close to the fiber surface and decays through the thickness. Contraction along the director decreases with decreasing temperature, and the fiber bends towards the surface of greatest strain. When the laser is turned off, the fiber cools as heat is transferred away and it relaxes back to its initial conformation. The observed, reversible bending in response to light and relaxation in the dark confirms that photothermal heat generation from the AuNPs is sufficient to drive actuation at room temperature.

Following confirmation of the photoresponse due to flood actuation, we explored the actuation in response to waveguided light. A PMMA polymer optical fiber (POF) patch cord of 500 μm in diameter with the jacket at the end of the cord removed was used to couple the laser to the end of the nanocomposite fiber. The underside of the LCE fiber was attached to a glass slide by double

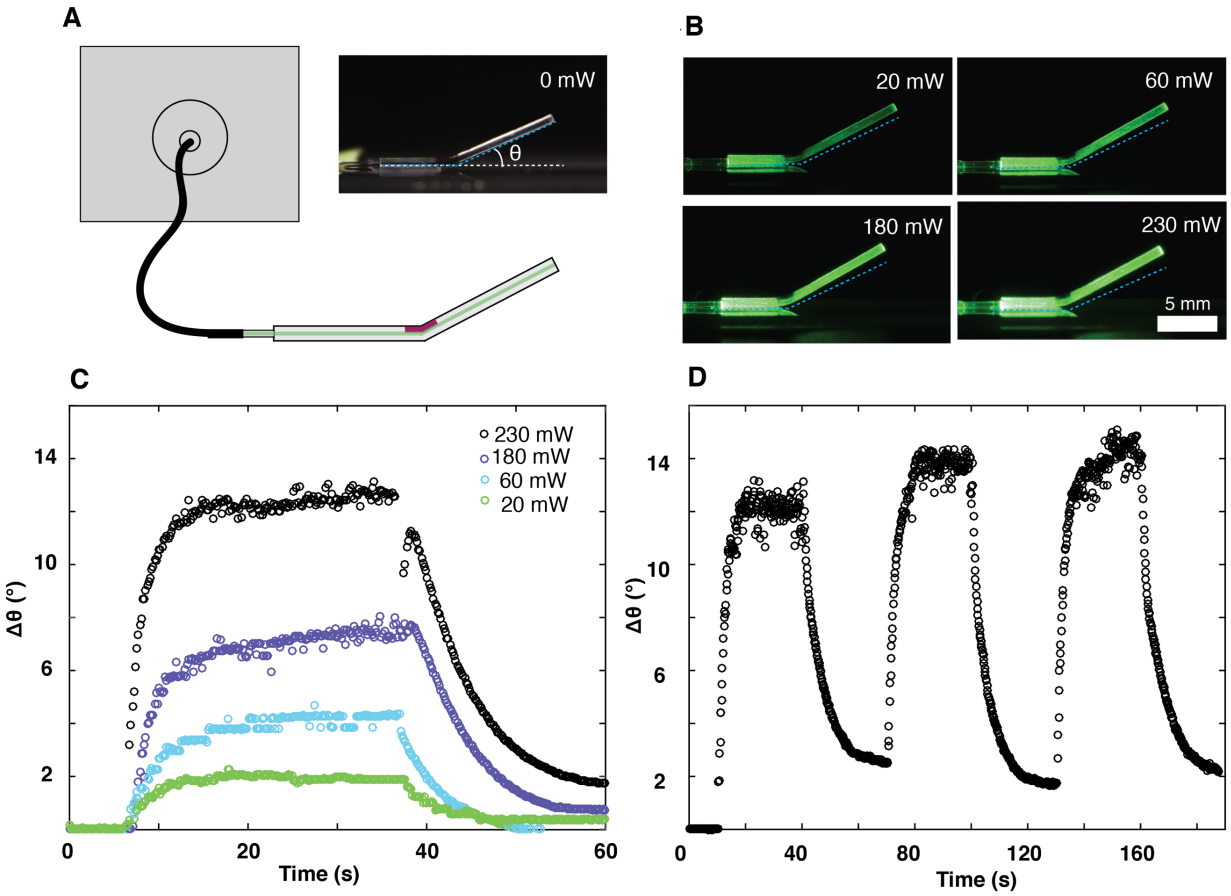

Figure 2. A) Schematic of an LCE waveguide couple to a DPSS laser via a PMMA waveguide (left) and a photograph of the initial waveguide configuration before illumination (right). The initial bend angle is due to a slight gradient in order parameter through the thickness of the fiber after swelling with gold salt. B) Photographs of steady state bend angle under different laser intensities. C) Actuator response during 30 s of waveguided illumination at different laser intensities. The laser is turned on at 8 s and turned off at 38 s. The bending angle increases with increasing light intensity due to greater photothermal heat generation and relaxes back to nearly its original position over a few seconds when the laser is turned off. D) Repeated actuation during illumination cycles of 30 s on/30 s off.

sided tape and a microscope was used to align the end of the fiber with the POF, after which the POF was taped to the glass substrate to hold it in place. To evaluate its light-induced bending behavior the fiber was exposed to 0.017 Hz illumination cycles (30s on / 30s off) at varying light intensities (**Figure 2**). When the light is turned on, the bend angle smoothly increases to a constant angle which is held until the light is turned off and the fiber relaxes continuously to its initial conformation. As the light intensity increased, the change in bending angle also increased

due to more extensive heat generation, with up to a 13º bend angle observed for a maximum intensity of 230 mW (**Figure 2**a); this behavior was repeatable over several cycles (**Figure 2**b). We note that the attainment of a constant bend angle while the light is on indicates that thermal steady state is achieved, and that it is characterized by a sufficient thermal gradient across the fiber diameter to drive bending. We note that this requires heat transfer out of the fiber to be appreciable—if the fiber were perfectly insulated, the temperature would continue to increase over time, ultimately leading to a nearly uniform contraction of the fiber, rather than localized bending. A coarse (order-of-magnitude) estimate of the steady-state temperature increase can be made as follows. Assuming that 10% of the laser power is absorbed by particles in a given actuator yields a total heat generation of q = 0.02 W. Simplifying the problem to conduction in an infinite medium, with a typical thermal conductivity (k) value for the polymer fiber of 0.2 W m^{-1} K^{-1} , the temperature increase at the edge of an actuator with characteristic size l = 1 mm can be estimated as $\Delta T \approx q/(4\pi kl) \approx 10$ K. From the data in Fig. 1B, we note that this would correspond to differences in strain across the fiber of several percent, consistent with the modest changes in radius of curvature, relative to the fiber radius, observed during photo-actuation.

As shown in **Figure 3**b, the incident laser light can be observed along the length of the fiber due to scattering losses, with a substantial decrease in intensity following the AuNP region due to absorption. Additionally, scattering can be observed at the tip of the LCE fiber, indicating that at least some portion of the light is guided through the entire length of the cm-scale device. Using UV-vis spectroscopy to measure the transmittance of a planar sample of known thickness with uniform in-plain director orientation (and correcting for reflection; see Supporting Information for details), we estimate an optical loss in the LCE materials as ~ 10 dB cm^{-1}, which is most

likely dominated by scattering from defects in the ordering of the mesogens. While the samples are globally oriented, the presence of interfaces between micrometer-scale domains with slightly different orientation can give rise to substantial scattering of light.[46] However, given that appreciable light intensities are still present even towards the end of cm-scale devices, we suspect this value to be an over-estimate of the real losses in the fiber, perhaps due to the difference in mesogen orientation relative to the direction of light propagation in the two cases. In future work, it will be important to evaluate the optical losses of these materials in greater detail. In particular, we anticipate that it may be possible to reduce the relatively high losses of current devices through improvements in ordering of the LCE fiber. For reference, optical fibers with small molecule LC cores have shown losses of ~1 dB cm^{-1} for highly oriented mesophases [47]. Although we expect that monodomain LCEs will generally have higher optical losses than their small molecule counterparts, due to the presence of non-LC monomers and crosslinkers that can lower the order parameter, optimization of the fiber processing approach is likely to improve transmission substantially. However, for cm-scale devices such as those demonstrated here, even such large losses do not preclude a robust photomechanical response.

To characterize the actuation kinetics, single exponential curves were fit to the data on bend angle vs. time after turning the laser on and off. Upon illumination, the fiber bent with a time constant of 3.3 s and when the light was turned off, the fiber relaxed with a time constant of 7.7s. While the bending kinetics of the LCE fiber are similar to those previously reported for waveguiding actuators based on hydrogels,[27] the backwards kinetics are several-fold faster. These timescales are consistent with the expected timescale for heat transfer, roughly estimated as $\tau \sim 5$ s from $\tau \sim d^2/D_t$ where $D_t \sim 10^{-7}$ m^2/s is a typical value of thermal diffusivity for a polymer matrix.[48] While

heat transfer effects alone could conceivably account for the observed differences in the forward and backward kinetics, it is also possible that viscoelastic properties could play a role in setting the actuation timescale. Further study is required to fully understand these effects.

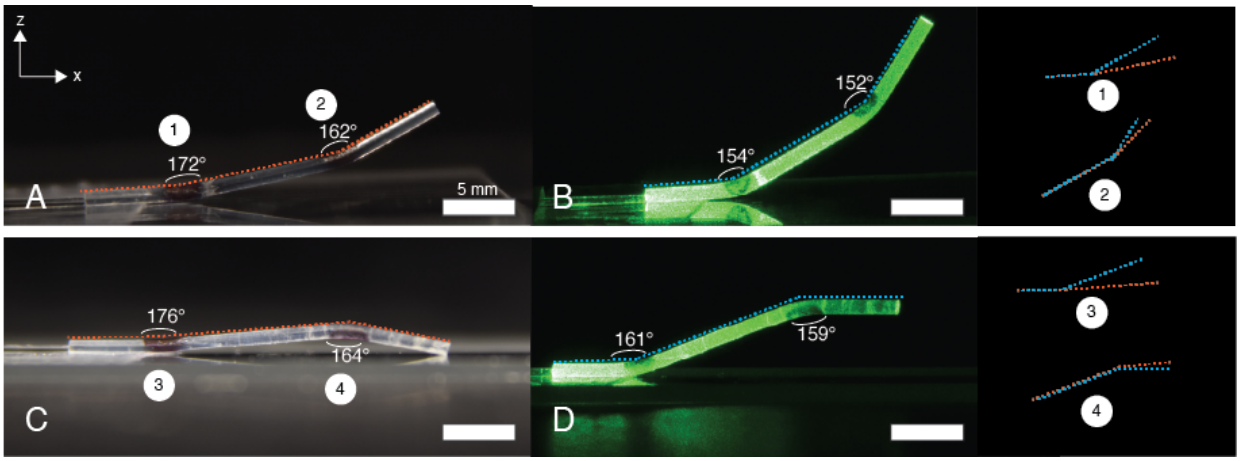

Figure 3. Deformation of a fiber containing two actuators. (A) Side view of a fiber containing two actuators fabricated on top of the fiber before illumination. (B) When the light is turned on, the fiber bends by 18° and 10° at actuators 1 and 2, respectively. (C) Side view of a fiber containing two actuators fabricated on opposite sides of the fiber (180° offset) before illumination. (D) When the light is turned on, the fiber bends up by 15° at actuator 3 and down by 5° at actuator 4. Stick diagrams on the far right show the overlay of each hinge with and without light stimulation for ease of viewing.

Multiple bends in a single fiber can be achieved by depositing several droplets of gold precursor solution at different positions along the same fiber. For example, the responses of fibers containing two discrete actuators are shown in **Figure 3**. In **Figure 3**a, the actuators contain nanoparticles on the same side of the fiber with no offset in azimuthal position. To mitigate the effects of decreasing light intensity along the length of the fiber due to absorbance by the first actuator and scattering losses, the second actuator was fabricated with double the exposure time to increase its absorbance relative to the first actuator. When the light was guided through the fiber as shown in **Figure 3**b, the first actuator bent by 18° and the second actuator by 10° along the +z axis. However, when the actuators were azimuthally offset by 180º, bending along both the +z and –z direction was achieved

(**Figure 3**c-d). In this configuration, the fiber bent upwards by 15° at the first actuator and downwards by 5° at the second (**Figure 3**d).

Finally, bending along multiple different axes within the same fiber was realized, as shown in **Figure 4**. Three discrete actuators were fabricated with increasing absorbance and separated by ~ 5 mm each, as can be seen by the side-view in **Figure 4**a. Actuator 1 was located on the top of the fiber, while actuators 2 and 3 were offset by +90° and -90°, respectively. As evidenced by **Figure 5**b, when the light was turned on, the fiber bent upwards along the +z direction at the first actuator but not along actuators 2 and 3. When viewed from the top, as shown in **Figure 4**c and **Figure 4**d, the fiber is shown to have bent in the +y and –y directions at actuators 2 and 3, respectively. The fiber bent by a decreasing degree as the light traveled down the length of the fiber with bend

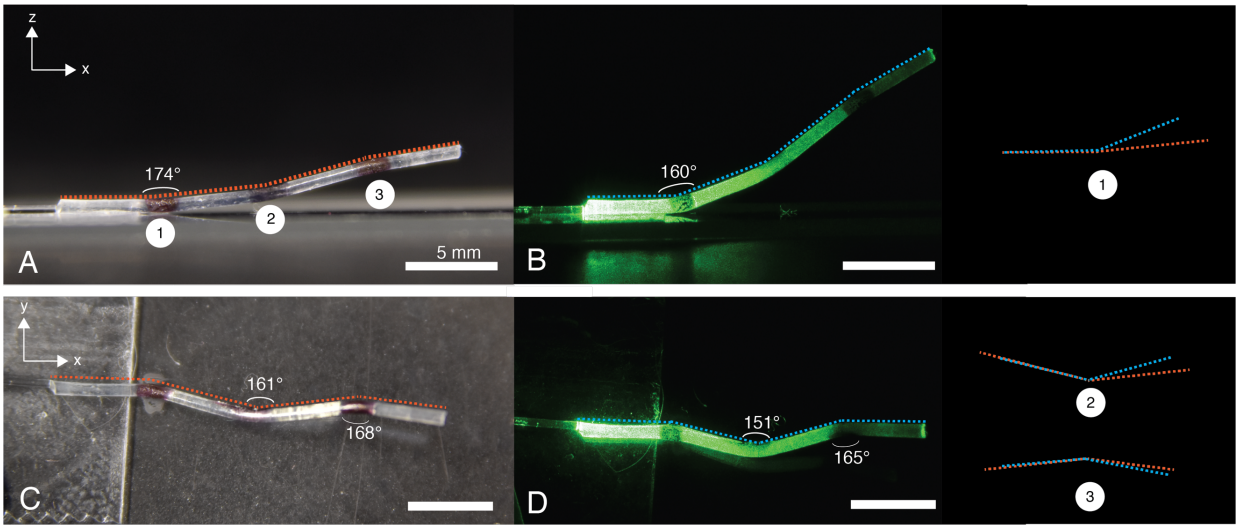

Figure 4. Deformation of an optical fiber containing three actuators. (A) Side view with the light off. Actuator 1 corresponds to nanoparticles placed on the top of the fiber and actuators 2 and 3 correspond to nanoparticles placed on opposite sides of the fiber, each offset 90° from actuator 1, and 180° from each other. (B) Side view with the light on shows that actuator 1 bends 14° under light stimulation. (C) Top view with the light off. (D) Top view with the light on showing that actuator 2 and 3 bend the fiber in opposite directions by 10° and 3°, respectively. Stick diagrams on the far right show the overlay of each hinge with and without light stimulation for ease of viewing.

angles of 14°, 10°, and 3° for actuators 1, 2, and 3, respectively, due to decaying intensity as can be observed in the photograph in **Figure 4**.

In conclusion, we have demonstrated the fabrication of photothermal actuators amenable to control via waveguided light using an LCE nanocomposite system. Photoresponsive regions can be precisely defined via photoreduction of gold salt to drive bend angles of > 14º on the timescale of seconds. Furthermore, bending in multiple directions can be achieve through judicious choice of nanoparticle placement and can be used to program bending into three-dimensional conformations with arbitrary placement and direction of bends upon deployment. Finally, this method provides a means to control the device in situation where line-of-sight access is not feasible and waveguiding removes the need to synchronize the location of the light source in free space with that of the actuators.

Experimental Section

Materials: Pentaerythritol tetrakis(3-mercaptopropionate) (PETMP), 2,2-(ethylenedioxy) diethanethiol (EDDET), 2,2-dimethoxy-2-phenyl-acetophenone (Irgacure 651), dipropylamine (DPA), gold(III) chloride trihydrate ($HAuCl_4$), and oleylamine where purchased from Sigma Aldrich and used without further purification. The diacrylate mesogen 1,4-Bis-[4-(3-acryloyloxypropyloxy)benzoyloxy]-2-methylbenzene (RM257) was purchased from Wilshire Technologies and used as received.

LCE Fiber Synthesis and Fabrication: The procedure of Yakacki *et al*. [35] was used with slight modifications. RM257 (0.5 g), EDDET (0.12 g), PETMP (0.024 g), and Irgacure 651 (3 mg) were dissolved in toluene (420 µL) under gentle heating with a heat gun. After the solids were fully dissolved, the solution was cooled to room temperature and DPA (1.5 µL) was added. Finally, the solution was degassed under vacuum, filled into cylindrical silicone molds, and left to cure in the dark at RT for 12 h. Following gelation, the clear gel preforms were dried under vacuum at 50 ºC for several hours to yield opaque white fibers. The dried fibers were placed under 200% strain using a homemade stretching device and polymerized under UV light for 10 min (90 mW cm^{-2}).

Gold Nanoparticle Patterning: The gold precursor solution was prepared by sequentially combining $HAuCl_4$ (200 µL of 0.1 M in acetone), Irgacure 651 (400 µL of a 0.5 M solution in toluene), and oleylamine (200 µL of a 0.3 M solution in toluene) in a pre-cleaned vial. Upon addition of the oleylamine, the bright yellow solution became clear and was aged for 1 h to yield a pale brown solution. Following aging, 1 µL droplets were deposited on the surface of the fiber

and covered to prevent evaporation of the toluene/acetone mixture. After several minutes, the droplet locally swelled the preform, as evidenced by a slight bend in the fiber and the appearance of an opaque bump where the droplet was deposited. To initiate particle formation, UV light was focused on the surface of the fiber where the gold salt was deposited using a DMD (DLP Discovery 4100, .7 XGA, Texas Instruments) attached to an inverted optical microscope (Nikon ECLIPSE Ti) in increments of 60s depending on the desired absorbance. An advantage of this approach compared to the use of a more conventional UV source is that it avoids significant heating of the sample, providing better defined patterns of Au NPs. After UV exposure, the fibers were dried under vacuum to remove residual solvent.

Instruments and Measurements: Absorbance of the AuNPs was measured using a UV-vis spectrophotometer (Hitachi, U-3010) with planar LCE sample geometries prepared by a similar method as above. Order parameters were calculated from wide-angle X-ray scattering collected using a GANESHA 300 XL (SAXSLAB) by numerically integrating in MATLAB

$$S = 1 - N^{-1}\frac{3}{2}\int_0^{\pi/2} I(\theta)\left[\sin^2\theta + (\sin\theta + \cos^2\theta)log\frac{1+\sin\theta}{\cos\theta}\right]d\theta$$

where $N = \int_0^{\pi/2} I(\theta)d\theta$.[49] Deformation of the fibers was measured by heating a small sample of an aligned fiber in silicone oil on a silicon substrate on a heat stage (Instec), images were taken using an upright microscope (Zeiss, Axiotech Vario) outfitted with a camera (Pixelink), and length change was measured using ImageJ software. Photoactuation experiments were conducted using a 532 nm DPSS laser (Laserglow) the intensity of which was controlled using absorptive neutral density filters (Thorlabs). Laser light was delivered to the LCE fiber through a 500 μm diameter

FC terminated POF with a PMMA core. A camera (Nikon 5500) was used to monitor the photoresponse and bending angle was measured using Tracker software (Open Source Physics). For flood actuation experiments, a fiber was placed in water to provide heat dissipation and illuminated by bringing the tip of the POF attached to the laser close to the nanoparticle region of an LCE actuator. For waveguiding experiments, the cladding was removed from the end of the POF and the tip was butt coupled to the LCE actuator by fixing the POF and LCE in place using a piece of double-sided tape and mechanically aligning the fibers to maximize light transmission.

Supporting Information

Supporting Information is available from the Wiley Online Library or from the author.

Acknowledgements

Support for this work was provided by the National Science Foundation through EFRI-ODISSEI 1332271, with additional support from the Office of Naval Research through the MURI on Photomechanical Materials (ONR N00014-18-1-2624). The authors thank Y. Zhou for assistance with the actuation experiments.

Received:

Revised:

Published online:

References

[1] T. J. White, *Photomechanical Materials, Composites, and Systems: Wireless Transduction*

of Light Into Work, John Wiley & Sons, Ltd., Hoboken, **2017**.
[2] Y. Yu, M. Nakano, T. Ikeda, *Nature* **2003**, *425*, 145.
[3] H. Finkelmann, E. Nishikawa, G. G. Pereira, M. Warner, *Phys. Rev. Lett.* **2001**, *87*, 1.
[4] S. K. Ahn, T. H. Ware, K. M. Lee, V. P. Tondiglia, T. J. White, *Adv. Funct. Mater.* **2016**, *26*, 5819.
[5] S. Iamsaard, S. J. Aßhoff, B. Matt, T. Kudernac, J. J. L. M. Cornelissen, S. P. Fletcher, N. Katsonis, *Nat. Chem.* **2014**, *6*, 229.
[6] C. J. Barrett, J. Mamiya, K. G. Yager, T. Ikeda, *Soft Matter* **2007**, *3*, 1249.
[7] R. O. Al-Kaysi, A. M. Müller, C. J. Bardeen, *J. Am. Chem. Soc.* **2006**, *128*, 15938.
[8] T. Kim, L. Zhu, R. O. Al-Kaysi, C. J. Bardeen, *ChemPhysChem* **2014**, *15*, 400.
[9] D. Corbett, C. Xuan, M. Warner, *Phys. Rev. E - Stat. Nonlinear, Soft Matter Phys.* **2015**, *92*, 8.
[10] T. Kim, L. Zhu, L. J. Mueller, C. J. Bardeen, *J. Am. Chem. Soc.* **2014**, *136*, 6617.
[11] E. Wang, M. S. Desai, S. W. Lee, *Nano Lett.* **2013**, *13*, 2826.
[12] A. W. Hauser, A. A. Evans, J. H. Na, R. C. Hayward, *Angew. Chemie - Int. Ed.* **2015**, *54*, 5434.
[13] J. Ryu, M. D'Amato, X. Cui, K. N. Long, H. Jerry Qi, M. L. Dunn, *Appl. Phys. Lett.* **2012**, *100*, DOI 10.1063/1.3700719.
[14] Y. Liu, B. Shaw, M. D. Dickey, J. Genzer, *Sci. Adv.* **2017**, *3*, 1.
[15] A. W. Hauser, D. Liu, K. C. Bryson, R. C. Hayward, D. J. Broer, *Macromolecules* **2016**, acs. macromol.6b00165.
[16] A. H. Gelebart, D. Jan Mulder, M. Varga, A. Konya, G. Vantomme, E. W. Meijer, R. L. B. Selinger, D. J. Broer, *Nature* **2017**, *546*, 632.
[17] J. E. Marshall, Y. Ji, N. Torras, K. Zinoviev, E. M. Terentjev, *Soft Matter* **2012**, *8*, 1570.
[18] M. G. Kuzyk, *Polymer Fiber Optics: Materials, Physics, and Applications*, CRC Press, Boca Raton, **2007**.
[19] D. J. Welker, M. G. Kuzyk, *Appl. Phys. Lett.* **1994**, *64*, 809.
[20] D. J. Welker, M. G. Kuzyk, *Appl. Phys. Lett.* **1996**, *69*, 1835.
[21] S. Bian, D. Robinson, M. G. Kuzyk, *J. Opt. Soc. Am. B* **2005**, *23*, 13.
[22] X. Ye, M. G. Kuzyk, *Opt. Commun.* **2014**, *312*, 210.
[23] Y. Otani, Y. Hirai, Y. Mizutani, N. Umeda, T. Yoshizawa, *Proc. SPIE* **2006**, *6376*, 63740N.
[24] Y. Otani, Y. Matsuba, *Proc. SPIE* **2001**, *4564*, 216.
[25] K. Zinoviev, C. Dominguez, J. A. Plaza, L. M. Lechuga, *Appl. Phys. Lett.* **2008**, *92*, 2006.
[26] W. Small IV, T. S. Wilson, W. J. Benett, J. M. Loge, D. J. Maitland, *Opt. Express* **2005**, *13*, 8204.
[27] Y. Zhou, A. W. Hauser, N. P. Bende, M. G. Kuzyk, R. C. Hayward, *Adv. Funct. Mater.* **2016**, *26*, 5447.
[28] J. Naciri, A. Srinivasan, H. Jeon, N. Nikolov, P. Keller, B. R. Ratna, *Macromolecules* **2003**, *36*, 8499.
[29] C. Ohm, M. Morys, F. R. Forst, L. Braun, A. Eremin, C. Serra, R. Stannarius, R. Zentel, *Soft Matter* **2011**, *7*, 3730.
[30] T. Yoshino, J. Mamiya, M. Kinoshita, T. Ikeda, Y. Yu, *Mol. Cryst. Liq. Cryst.* **2010**, *478*, 233.
[31] L. Yu, H. Shahsavan, G. Rivers, C. Zhang, P. Si, B. Zhao, *Adv. Funct. Mater.* **2018**, *28*, 1802809.

[32] A. H. Gelebart, M. Mc Bride, A. P. H. J. Schenning, C. N. Bowman, D. J. Broer, *Adv. Funct. Mater.* **2016**, *26*, 5322.
[33] L. Fang, G. Han, J. Zhang, H. Zhang, H. Zhang, *Eur. Polym. J.* **2015**, *69*, 592.
[34] S. Nocentini, D. Martella, D. S. Wieserman, C. Parmeggiani, *Soft Matter* **2017**, *13*, 8590.
[35] C. M. Yakacki, M. Saed, D. P. Nair, T. Gong, S. M. Reed, C. N. Bowman, *RSC Adv.* **2015**, *5*, 18997.
[36] M. O. Saed, A. H. Torbati, C. A. Starr, R. Visvanathan, N. A. Clark, C. M. Yakacki, *J. Polym. Sci. Part B Polym. Phys.* **2017**, *55*, 157.
[37] A. H. Gelebart, G. Vantomme, E. W. Meijer, D. J. Broer, *Adv. Mater.* **2017**, *29*, DOI 10.1002/adma.201606712.
[38] K. L. McGilvray, M. R. Decan, D. Wang, J. C. Scaiano, *J. Am. Chem. Soc.* **2006**, *128*, 15980.
[39] a S. Korchev, M. J. Bozack, B. L. Slaten, G. Mills, *J. Am. Chem. Soc.* **2004**, *126*, 10.
[40] M. L. Marin, K. L. McGilvray, J. C. Scaiano, *J. Am. Chem. Soc.* **2008**, *130*, 16572.
[41] H. Hiramatsu, F. E. Osterloch, *Chem. Mater.* **2004**, *16*, 801.
[42] J. D. S. Newman, G. J. Blanchard, *Langmuir* **2006**, *22*, 5882.
[43] M. Aslam, L. Fu, M. Su, K. Vijayamohanan, V. P. Dravid, *J. Mater. Chem.* **2004**, *14*, 1795.
[44] N. K. Singh, A. J. Lesser, *Macromolecules* **2011**, *44*, 1480.
[45] T. Twardowski, O. Kramer, *Macromolecules* **1991**, *24*, 5769.
[46] S. M. Clarke, E. M. Terentjev, I. Kundler, H. Finkelmann, *Macromolecules* **1998**, *31*, 4862.
[47] D. C. Zografopoulos, R. Asquini, E. E. Kriezis, A. D'Alessandro, R. Beccherelli, *Lab Chip* **2012**, *12*, 3598.
[48] M. Harada, M. Ochi, M. Tobita, T. Kimura, T. Ishigaki, N. Shimoyama, H. Aoki, *J. Polym. Sci. Part B Polym. Phys.* **2003**, *41*, 1739.
[49] M. Deutsch, *Phys. Rev. A* **1991**, *44*, 8264.